Brain Topogr (2014) 27:747–765
DOI 10.1007/s10548-014-0357-7

ORIGINAL PAPER

Identifying and Characterizing Resting State Networks in Temporally Dynamic Functional Connectomes

Xin Zhang · Xiang Li · Changfeng Jin · Hanbo Chen · Kaiming Li · Dajiang Zhu · Xi Jiang · Tuo Zhang · Jinglei Lv · Xintao Hu · Junwei Han · Qun Zhao · Lei Guo · Lingjiang Li · Tianming Liu

Received: 27 September 2013 / Accepted: 14 February 2014 / Published online: 6 June 2014

Abstract An important application of resting state fMRI data has been to identify resting state networks (RSN). The conventional RSN studies attempted to discover consistent networks through functional connectivity analysis over the whole scan time, which implicitly assumes that RSNs are static. However, the brain undergoes dynamic functional state changes and the functional connectome patterns vary along with time, even in resting state. Hence, this study aims to characterize temporal brain dynamics in resting state. It utilizes the temporally dynamic functional connectome patterns to extract a set of resting state clusters and their corresponding RSNs based on the large-scale consistent, reproducible and predictable whole-brain reference system of dense individualized and common connectivity-based cortical landmarks (DICCCOL). Especially, an effective multi-view spectral clustering method was performed by treating each dynamic functional connectome pattern as one view, and this procedure was also applied on static multi-subject functional connectomes to obtain the static clusters for comparison. It turns out that some dynamic clusters exhibit high similarity with static clusters, suggesting the stability of those RSNs including the visual network and the default mode network. Moreover, two motor-related dynamic clusters show correspondence with one static cluster, which implies substantially more temporal variability of the motor resting network. Particularly, four dynamic clusters exhibited large differences in comparison with their corresponding static networks. Thus it is suggested that these four networks might play critically important roles in functional brain dynamics and interactions during resting state, offering novel insights into the brain function and its dynamics.

Keywords Resting state network (RSN) · Brain dynamics · DICCCOL · Structural connectome · Functional connectome

Xin Zhang, Xiang Li and Changfeng Jin contributed equally to this work.

Electronic supplementary material The online version of this article (doi:10.1007/s10548-014-0357-7) contains supplementary material, which is available to authorized users.

X. Zhang · K. Li · T. Zhang · J. Lv · X. Hu · J. Han · L. Guo
School of Automation, Northwestern Polytechnical University, Xi'an, China

X. Zhang · X. Li · H. Chen · K. Li · D. Zhu · X. Jiang · T. Zhang · J. Lv · T. Liu (✉)
Cortical Architecture Imaging and Discovery Lab, Department of Computer Science and Bioimaging Research Center, The University of Georgia, Athens, GA, USA
e-mail: tliu@cs.uga.edu; tianming.liu@gmail.com

C. Jin · L. Li (✉)
The Mental Health Institute, The Second Xiangya Hospital of Central South University, Changsha, China
e-mail: llj2920@163.com

Q. Zhao
Department of Physics and Astronomy and Bioimaging Research Center, The University of Georgia, Athens, GA, USA

Introduction

The human brain can be considered as a complex integrative network, constituted by a set of spatially distributed but functionally related brain regions that communicate with each other. In recent years, the application of resting state fMRI (R-fMRI) technique has generated a great deal of research interest in investigating the characteristics of the human brain in a baseline state, among which an interesting topic is to discover the functional resting state networks (RSN) (e.g., Lowe et al. 1998; De Luca et al. 2005; Van den Heuvel et al. 2008).

Table 1 The numbers of clusters according to different N-cut thresholds

N-cut threshold	0.05	0.1	0.2	0.3	0.4	0.5
Number of dynamic clusters (multi-pattern)	9	9	10	10	10	10
Number of static clusters (multi-subject)	6	8	8	8	8	9

Towards this goal, the low-frequency fluctuations (0.01–0.1 Hz) in the blood oxygenation level-dependent (BOLD) signal of resting state fMRI (R-fMRI) data (Damoiseaux et al. 2006; De Luca et al. 2006) received intense attention. It is commonly believed to date that the resting state fluctuations can reflect the spontaneous neuronal activity and the correlation of the fluctuations is a manifestation of the ongoing functional connectivity during rest (e.g., Biswal et al. 1995; Lowe et al. 1998; Cordes et al. 2000). Consequently, a set of functional brain regions involved in visual, motor, language and auditory functions were identified as distinct resting state networks (RSNs) by looking into the coherent low frequency fluctuations among different brain areas (e.g., Hampson et al. 2004; Beckman et al. 2005; De Luca et al. 2006; Damoiseaux et al. 2006; Van den Heuvel et al. 2008; Smith et al. 2012). Especially, a cohesive baseline network termed default mode network (DMN) (Raichle et al. 2001; Greicius et al. 2003) was discovered and reproduced, corresponding to task-independent introspection, i.e., it is active during rest but deactivated during specific goal-directed behaviors. This network may represent the underlying physiological processing of the brain unrelated to any particular thought (Raichle and Snyder 2007) and has been hypothesized to be associated with some neural disorders such as Alzheimer's disease, autism and schizophrenia (e.g., Greicius et al. 2004; Buckner et al. 2008; Assal et al. 2010).

The current resting state network analysis methods mainly employed the conception of functional connectivity to describe the temporal dependency of neural activation patterns or co-activation levels of R-fMRI time series between distinct brain regions (e.g., Aertsen et al. 1989; Friston et al. 1993; Biswal et al. 1995; Lowe et al. 1998; Cordes et al. 2000; Calhoun et al. 2001; Cordes et al. 2012; Greicius et al. 2003; Jiang et al. 2004; Beckman et al. 2005; De Luca et al. 2006; Damoiseaux et al. 2006; Thirion et al. 2006; Van den Heuvel et al. 2008; Larson-Prior et al. 2009). Basically, this definition of functional connectivity is assumed to be temporally static, i.e., the calculation of connectivity is performed over the entire fMRI scan period. Whereas one recent study proposed and demonstrated that the function of each brain area is not fixed or stereotyped (Gilbert and Sigman 2007). Instead, each area works as an adaptive information processor; they attempt to execute different programs or algorithms according to the behavioral context and the perceptual requirements (Gilbert and Sigman 2007). Therefore this kind of dynamic processing will result in a whole-brain moment-to-moment functional switching mode, and furthermore the brain will be very likely to exhibit various function connectome patterns at different time periods. Encouragingly, it has been evidenced that the human brain indeed undergoes dynamic function connectivity changes within the scan period, even in resting state (e.g., Chang and Glover 2010; Zhang et al. 2012; Smith et al. 2012; Li et al. 2013; Zhang et al. 2013). In the literature, several methodologies have also been developed to investigate connectivity dynamics, including sliding-time window correlation analysis with reference vector (Gembris et al. 2000), dynamic spatial independent component analysis (ICA) (Sakoğlu et al. 2010), and analysis using sliding-time window correlation between connectivity networks obtained from spatial ICA (Allen et al. 2014). In particular, our own prior studies suggested that the dynamic brain states can be expressed by a set of whole-brain functional connectome patterns in resting state or task-performance for normal subjects or diseased brains at different time periods (Zhang et al. 2012, 2013; Li et al. 2013). The abovementioned series of studies have demonstrated that computational modeling of functional brain dynamics has revealed important novel insights that cannot be seen by conventional static functional connectivity analysis methods. However, an important and yet unanswered question is: among the commonly reported RSNs, which ones exhibit more temporal dynamics than others? In other words, which RSNs exhibit more temporal dynamics, or less temporal stationarity, than others?

Motivated by the above question, this paper presents a novel computational framework to identify RSNs in temporally dynamic functional connectomes and to characterize their temporal dynamics specifically. Compared to the previous analysis methods (e.g., Gembris et al. 2000; Sakoğlu et al. 2010; Allen et al. 2014; Chang and Glover 2010; Zhang et al. 2012; Smith et al. 2012), it mainly has the following novelties. (1) It adopted a whole-brain functional connectivity map based on a recently developed and validated brain reference system of 358 dense individualized and common connectivity-based cortical landmarks (DICCCOLs) (Zhu et al. 2012; Yuan et al. 2012; Li et al. 2013; Zhang et al. 2013). It has been shown that the 358 DICCCOLs have structural and functional correspondences across individuals and populations. Importantly, they can be reproduced and predicted across different brains through an effective predicting method (Zhu et al. 2012). This system has been successfully used to characterize dynamic brain states for both resting state and task-performance brains in our previous works (Zhang et al. 2012, 2013). (2) Based on the dynamic whole-brain functional connectivity change curves obtained by the sliding time window approach, this framework employed a sparse coding based classification method to refine and extract a set of

Table 2 The cluster similarity (Eq. 9) between dynamic multi-pattern clusters (D1, D2,…, D10) and static multi-subject clusters (S1, S2,…, S10)

	S1	S2	S3	S4	S5	S6	S7	S8
D1	**0.937**	0.000	0.047	0.000	0.018	0.000	0.000	0.000
D2	0.000	**0.895**	0.000	0.028	0.000	0.000	0.000	0.000
D3	0.022	0.077	**0.888**	0.000	0.000	0.055	0.000	0.023
D4	0.024	0.000	0.000	**0.787**	0.017	0.116	0.000	0.024
D5	0.000	0.000	0.000	0.088	**0.691**	0.000	0.000	0.000
D6	0.000	0.000	0.000	0.000	0.000	**0.660**	0.070	0.030
D7	0.000	0.030	0.000	0.000	0.000	0.237	**0.645**	0.135
D8	0.000	0.000	0.000	0.000	**0.615**	0.000	0.000	0.000
D9	0.000	0.035	0.000	0.055	0.044	0.025	0.148	**0.559**
D10	0.000	0.000	0.028	0.109	0.066	0.223	0.000	**0.342**

For each dynamic cluster, the static cluster with the highest similarity (highlighted in bold) is considered as the corresponding cluster of this dynamic cluster

representative temporally dynamic functional connectome patterns of the brain (Zhang et al. 2012, 2013; Li et al. 2013). Each pattern can be finally represented here by a corresponding 358 × 358 connectivity matrix, which can be seen as one similarity matrix of 358 nodes in the spectral clustering methodology. (3) In comparison with our previous studies (Li et al. 2013; Zhang et al. 2013), an up-to-date effective spectral graph based multi-view clustering method is performed on these dynamic connectome patterns to group the 358 DICCCOLs into several sub-clusters, i.e., spatial networks (Bickel and Scheffer 2004; Chaudhuri et al. 2009; Kumar and Daumé, 2011). In this case, each cluster constitutes a RSN represented by a group of consistent DICCCOL landmarks. The multi-view co-training procedure attempts to achieve the most of the agreement *across* different 'views' (i.e. 'patterns') and achieve a more comprehensive and meaningful clustering result than traditional one-view clustering methods. In this study, after co-training on multiple temporally dynamic functional connectome patterns, a group composed of ten spatially distributed and relatively stable resting state DICCCOL clusters was formed. Moreover, for comparison, the static functional connectivity matrix for each subject was calculated based on the whole brain R-fMRI time series and a similar multi-view co-training procedure was applied to obtain another group of eight DICCCOL clusters. Experimental results have shown that some dynamic clusters exhibit high similarity with static clusters, indicating the stability of those RSNs including the visual and default mode networks. Interestingly, two motor-related dynamic clusters show correspondence with one static cluster, which suggests substantially more temporal dynamics of the motor resting network. Importantly, other four dynamic clusters exhibited substantial differences in comparison with their corresponding static networks, implying that these four networks might play critically important roles in functional brain dynamics and interactions during resting state. In general, our work in this study offers novel insights into the brain function and its dynamics.

Materials and Methods

Overview

The pipeline of our novel computational framework is summarized in Fig. 1. First, 358 large-scale DICCCOL landmarks (red bubbles in the left panel of Fig. 1) were predicted and located based on the DTI data through an effective functional landmark prediction approach (Zhu et al. 2012). Using the FSL FLIRT tool, each resting state fMRI data was co-registered to the corresponding DTI space and the R-fMRI time series in each DICCCOL were extracted (step ① in Fig. 1). Then, for each subject, a traditional static functional connectivity matrix can be measured by calculating the Pearson correlation coefficients between the corresponding R-fMRI time series of each pair of DICCCOLs over the entire scan period (step ⑤ in Fig. 1). However this matrix does not contain the vital information of temporal dynamics in resting state. Thus, we applied a sliding time window approach to measuring the dynamic functional connectivity matrices of each subject (step ② in Fig. 1). Subsequently, these matrices were segmented into smaller quasi-static time segments, called whole-brain quasi-stable connectome patterns (WQCP) in our prior paper (Zhang et al. 2012). Then a set of WQCP samples were collected as the input of the sparse representation based Fisher discriminative dictionary learning (FDDL) method (step ③ in Fig. 1). The FDDL classification results were finally represented by several averaged DICCCOL-based functional connectivity matrices associated with each class, i.e., the final expression of the temporally dynamic functional connectome patterns for resting state (step ④ in Fig. 1). Each pattern is a 358 × 358 functional connectivity matrix, which can be regarded as one view of the similarity matrix of the 358 DICCCOL nodes. Thus, an effective multi-view spectral clustering method was performed on these patterns (called multi-pattern clustering in this paper) to obtain a group of relatively consistent and spatially distributed clusters (step ⑥ in Fig. 1), i.e., resting state functional networks. Besides, the multi-view spectral clustering method can be similarly applied on the static functional connectivity matrix for each subject (step ⑤ in Fig. 1) by treating each static matrix as one view of the similarity matrix of 358 nodes (called

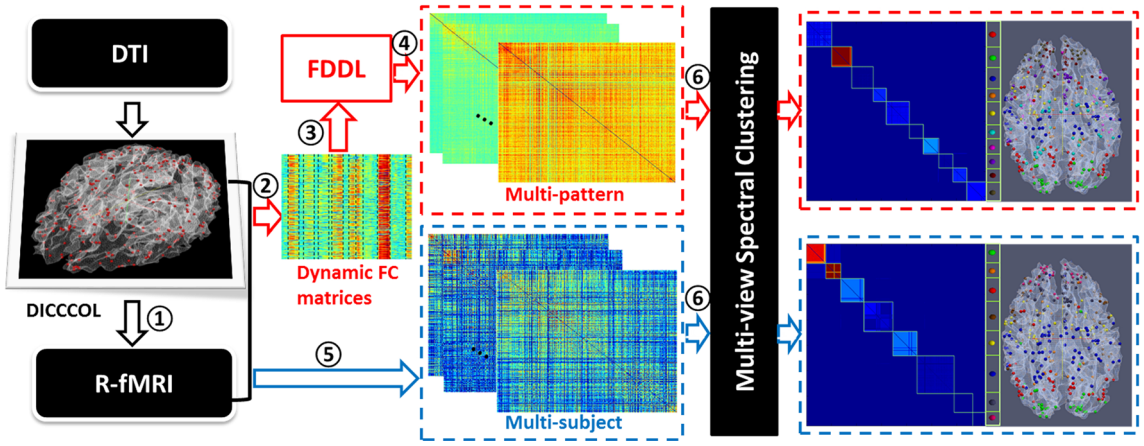

Fig. 1 The flowchart of our computational framework. ①: Extraction of DICCCOL R-fMRI signals. ②: Measurement of temporally dynamic functional connectivity matrices. ③: Acquisition and collection of WQCP samples. ④: FDDL classification and output of temporally dynamic functional connectome patterns. ⑤: Measurement of static functional connectivity matrix for each subject. ⑥: Multi-view spectral clustering for multiple patterns (dynamic) and multiple subjects (static) independently

multi-subject clustering in this paper) to achieve the static resting state clusters (⑥ in Fig. 1) for comparison.

Brief Introduction of DICCCOL

As indicated in our previous research, the structural connectome of each brain can be constructed by the dense map of 358 DICCCOL landmarks based on the DTI data (Zhu et al. 2012). One basic premise in the development of DICCCOL is that functional location can be predicted by group-wise consistent structural connectivity patterns (Zhu et al. 2012). Therefore, each DICCCOL landmark is defined and discriminated by different group-wise consistent white fiber streamline patterns, which were quantitatively described by the trace-map model (Zhu et al. 2012). Briefly, three steps were conducted to form the cortical DICCCOL map: the initial landmarks selection, the optimization of landmark locations and the determination of group-wise consistent DICCCOL landmarks. First, 2056 grid points/landmarks distributed among major functional brain regions were initially selected on one template subject, and then warped to other nine template subjects through a linear registration procedure. Subsequently, landmark locations were optimized to gain maximal group-wise consistent fiber connection patterns via the maximization of similarities of 'trace-map' models (Zhu et al. 2011). This model can capture the global shape patterns of fiber connections in each fiber bundle, based on which we can then measure and compare the similarities across fiber bundles. Essentially, the trace-map is a statistical accumulation of the projection points of the principal directions along the fiber trajectories in a fiber bundle onto a standard sphere space. The accumulation map is then normalized and mapped to a histogram that retains the global fiber shape to represent structural connectivity (Zhu et al. 2011). For each landmark of each subject, about 30 neighboring locations with corresponding emanating fiber bundles were selected as candidate landmark combinations and represented via trace-maps respectively. Then, each landmark is optimally selected through minimizing the energy function in Eq. 1, aiming to maximize the consistency of structural connection patterns across a group of template subjects.

$$E(S_1, S_2, \ldots, S_m) = \frac{\sum \sum_{i=1}^{n} (T_{ki} - T_{li})^2}{n}, k \neq l \text{ and } k, l = 1, 2, \ldots, m(1) \text{ and } k, l = 1, 2, \ldots, m \quad (1)$$

where S_1,…, S_m are m subjects; T_{ki} and T_{li} are the i-th element of trace-maps T_k and T_l respectively (Zhu et al. 2012). Furthermore, another group of subjects were analyzed using the same steps and the most consistent landmark locations were finally determined to form a dense map of 358 DICCCOL landmarks on each template cortical surface. The prediction procedure of DICCCOLs in other individual brains is also to solve an optimization problem like in Eq. (1). Specifically, first, this subject brain is mapped to the template brain to have an initial DICCCOL location map. Then, for each initialized landmark, the corresponding white matter fiber bundles of its candidate landmarks can be extracted and measured by trace-map. Subsequently, the prediction procedure is accomplished by selecting the optimal landmark from the candidates that has the least group-wise fiber connection variance compared to the corresponding DICCCOL landmarks in the template brains. Finally, a dense map of structural connectome of

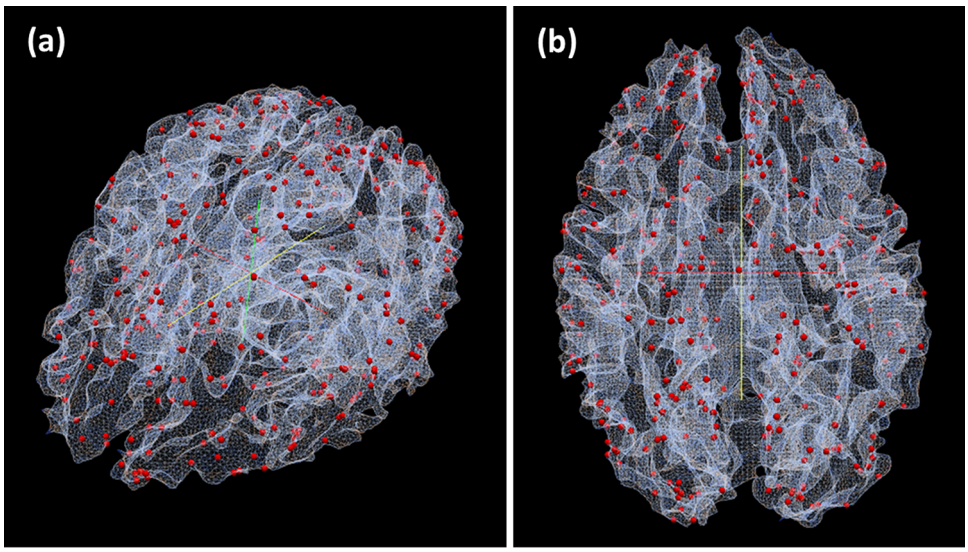

Fig. 2 358DICCCOL landmarks on the cortical surface. **a**, **b** are two different views

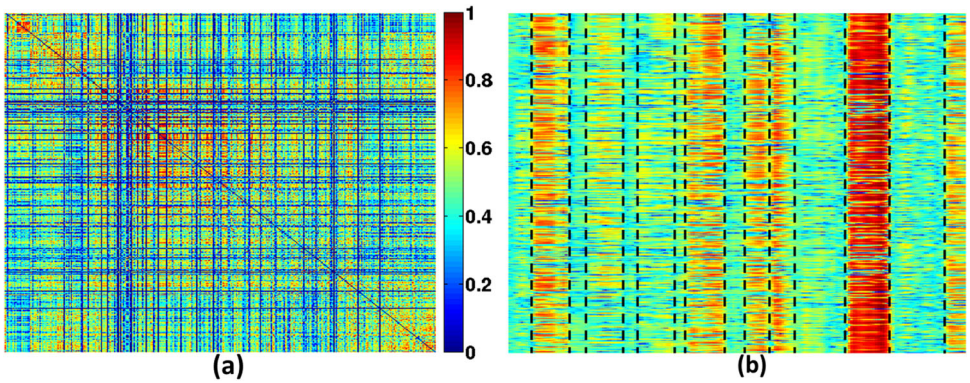

Fig. 3 **a** The DICCCOL-based static functional connectivity matrix of one resting state brain; **b** The DICCCOL-based temporally dynamic functional connectivity matrix of the same brain and its WQCPs

the new brain will be constructed and the fiber connection strength between each pair of DICCCOLs can be used as the connectome edge (Zhu et al. 2012). Figure 2 shows an example of the 358 DICCCOLs on a cortical surface.

Functional Connectomes

Temporally Static Functional Connectome Matrix

According to "Brief introduction of DICCCOL" section, the 358 DICCCOLs have structural and functional correspondences across individual brains, and especially, they can be reproduced and predicted on different brains. It provides a common and individualized brain reference system that serves as the structural substrate for functional connectome analysis. Based on this system, the functional connectome can be expressed by a graph composed of 358 DICCCOL nodes and the corresponding edges are weighted by the functional connectivity strengths between each pair of DICCCOLs.

Generally, the functional connectivity can be measured by the Pearson correlation coefficient between each pair of the R-fMRI time series extracted from the corresponding landmarks. In previous studies, researchers use the temporally static methods, i.e., obtain the time series correlation over the whole scan time period. In that case, the whole-brain functional connectome of each subject at rest can be represented by a 2D 358 $\times$ 358 functional connectivity matrix (Fig. 3a). In this matrix, the value of each element shows the intensity of the functional connection between the corresponding pair of DICCCOLs and the magnitude of the connectivity strength ranges from 0 to 1. Figure 3a shows an example of static functional connectivity matrix from a resting state brain. The horizontal axis and the vertical axis both indicate 358 DICCCOLs, as the matrix is symmetric. The functional connectivity strengths between each pair of DICCCOLs are color-coded according to the color bar on the right. Besides, the absolute values of Pearson correlation coefficients were adopted in correspondence with the subsequent temporally dynamic functional connectome analysis.

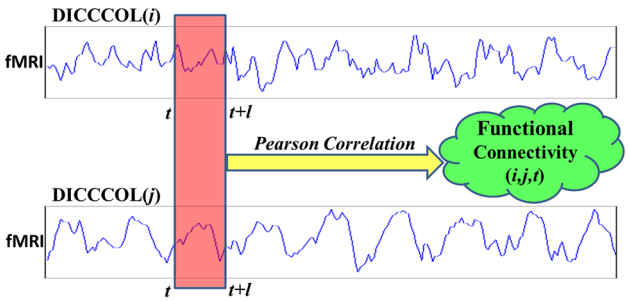

Fig. 4 The sliding time window approach to calculating the temporally dynamic functional connectivity matrices

Temporally Dynamic Functional Connectomes

The above-mentioned static whole-brain functional connectivity matrix is limited due to the lack of consideration of the temporal dynamics of the brain function. In fact, the brain undergoes remarkable dynamic functional processes at rest. Thus, this paper adopted a temporally dynamic whole-brain functional connectome pattern representation based on the DICCCOL reference system as follows.

Whole-Brain Quasi-Stable Connectome Patterns (WQCPs) As introduced in our previous work (Zhang et al. 2012), a set of whole-brain quasi-stable connectome patterns (WQCPs) were firstly extracted and collected from all of the participating subjects. First, a sliding time window was applied to obtain a series of windowed resting state fMRI time series for each DICCCOL at different time points as shown in Fig. 4. The window length was set to 14 in this work. The windowed R-fMRI signals for each landmark at each time point were then used to measure the functional connectivity between each pair of DICCCOLs within each corresponding time window using the Pearson correlation coefficient. Therefore, for each brain, a 3D 358 × 358 × (time windows) temporally dynamic functional connectivity matrix will be obtained. To obtain a more compact and intuitive representation of the brain functional connectome, the cumulative connectivity strength of each DICCCOL landmark is further measured by summing all the absolute values of functional connectivities between this landmark and all the other landmarks (Zhang et al. 2012), resulting in a corresponding 2D 358× (time windows) whole-brain temporally dynamic functional connectivity strength matrix. One example of this 2D strength matrix is given in Fig. 3b. The horizontal axis represents the time points and the vertical axis represents the 358 DICCCOL landmarks. It can be observed from this cumulative connectivity matrix that the connectivity strength keeps relatively stable in a continuous time period and we can segment WQCPs accordingly (illustrated by the black dash lines in Fig. 3b). For each WQCP segment, a WQCP vector (358 × 1) and its corresponding 2D connectivity matrix (358 × 358) can be obtained by time averaging. Subsequently, WQCPs from all of the resting state brains were pooled together and analyzed using the following classification method in order to achieve the representative whole-brain temporally dynamic functional connectome patterns in resting state.

Representative Whole-Brain Temporally Dynamic Functional Connectome Patterns The advantages of sparse representation approaches have been commonly recognized in a variety of image analysis applications including image classification (e.g., Yang et al. 2009, 2011; Wright et al. 2010; Zhang and Li 2010), image restoration (Mairal et al. 2008, 2009), image denoising (Elad and Aharon 2006) and image decomposition (Starck et al. 2005). Inspired by these successful applications, this paper adopts an effective sparse representation method called Fisher discriminative dictionary learning (FDDL) (Yang et al. 2011) to analyze the WQCP vector samples and extract the representative temporally dynamic functional connectome patterns. Briefly, the FDDL method employs a Fisher discrimination criterion to learn a structured dictionary. The learned dictionary is denoted by $D = [D_1, D_2,\ldots, D_c]$, where $D_i$is the sub-dictionary associated with class i, and c is the total number of learned classes. For each sample that has been determined to be belonging to class i, it would be represented by D_i. $A = [A_1, A_2,\ldots, A_c]$ represents the training samples and $A_i$is the sub-set of the training samples belonging to class i. $X = [X_1, X_2, \ldots, X_c]$represents the coding coefficient matrix of A over D (i.e. loadings of dictionary atoms). This methodology tries to achieve an optimal dictionary and a combination of optimal coding coefficients through independently updating the dictionary and the coding coefficients by solving the following equation during each iteration step in the learning procedure:

$$J_{(D,X)} = \arg\min_{(D,X)}\{r(A,D,X) + \lambda_1\|X\|_1 + \lambda_2 f(X)\} \quad (2)$$

The minimization function contains three items: $r(A, D, X)$is the discriminative fidelity term, making the dictionary D able to represent the data with minimum residual, while at the same time only using the correct sub-dictionary; $\|X\|_1$is the sparsity constraint; and the last term $f(X)$is a Fisher discrimination constraint imposed on the coefficient matrix. Detailed description of the dictionary learning algorithm could be found in Yang et al. 2009 and Li et al. 2013. λ_1 and λ_2 are scalar parameters for the trade-off between sparsity and discrimination capability. For our data, λ_1 was set to 0.005 and λ_2 was 0.05, which was experimentally determined to minimize the overall error

variance during training. The final classification procedure based on the learned dictionary is performed by finding the optimized $\widehat{\alpha}$ (coefficient) minimizing the representation error:

$$e_i = \left\| y - D_i\widehat{\alpha}_i \right\|_2^2 + w \cdot \left\| \widehat{\alpha} - m_i \right\|_2^2 \quad (3)$$

where $\widehat{\alpha} = [\widehat{\alpha}_1; \widehat{\alpha}_2; \ldots; \widehat{\alpha}_c]$ is the resulting sparse coding coefficient of the input test sample y using trained dictionary D obtained in Eq. (2), and $\widehat{\alpha}_i$is the coefficient vector associate with D_i; m_i is the learned mean vector of class i and w is a constant, which is set to 0.1 in this study.

The normalization procedure was performed on each WQCP vector sample to avoid the influence of individual connectivity strength differences. After FDDL classification, each WQCP vector sample was designed into one class in correspondence with one sub-dictionary. Specially, each WQCP vector is associated with a 358 × 358 DICCCOL-based functional connectivity matrix. Hence, the representative dynamic functional connectome pattern corresponding to each class can be represented by one 358 × 358 functional connectivity matrix through averaging all the WQCP matrices belonging to this class (Zhang et al. 2012, 2013; Li et al. 2013). The magnitude of each element in each matrix represents the functional connectivity strength between each DICCCOL pair in each pattern. As shown in Fig. 6, totally 8 temporal patterns were extracted from our resting state data. Deeper investigations into the dynamic resting-state temporal pattern will be of great significance, among which this study emphasizes on the spatial distribution of the resting state networks based on DICCCOL landmarks.

Identification of DICCCOL-Based Resting State Brain Networks

The concept of multi-view clustering has been recently employed in brain connectome analysis in our previous work, e.g., Chen et al. attempted to achieve group-wise structural and functional consistence of brain networks (Chen et al. 2013). In this study, a similar multi-view spectral clustering method was applied to the 8 temporally dynamic patterns obtained from the method described above to group the 358 spatially distributed DICCCOL landmarks into several spatial clusters, i.e., multi-pattern clustering, trying to identify consistent and stable dynamic resting state networks (Bickel and Scheffer 2004; Chaudhuri et al. 2009; Chen et al. 2013). In that case, DICCCOLs within each cluster may constitute a specific RSN and play a particular role in the resting-state functional activities.

Spectral Clustering

In this work, the 358 DICCCOL landmarks can be regarded as 358 input data points. The 358 × 358 functional connectome matrix from each temporal pattern or each subject can thus be seen as the similarity matrix of the data points, which is symmetric and non-negative. In general, spectral clustering is an effective way to cluster the 358 DICCCOLs into several sub-groups (Chen et al. 2013).

Generally we denote a weighted undirected similarity graph as $G = (V, E)$ with node set $V = \{v_1, \ldots, v_n\}$and edges set E connecting different nodes. The weight on each edge w_{ij} is a function of the similarity between nodes v_i and v_j, and the similarity matrix of the graph is denoted by $W = (w_{ij})_{i,j=1,\ldots,n}$, which is symmetric ($w_{ij} = w_{ji}$) and non-negative ($w_{ij} \geq 0$). The degree of a node v_i is defined as $d_i = \sum_{j=1}^{n} w_{ij}$. Then, the spectral clustering aims to seek the optimal partition of the graph into some node sub-groups $V_1, V_2, \ldots, V_k$, where by some measurement the similarity in the same sub-group is high enough, but between different sub-groups it is relatively low. To achieve this goal, a graph-theoretic criterion named normalized cut (N-cut) is introduced to measure the goodness of the partition criterion (Shi and Malik 2000; Chen et al. 2013). The definition of N-cut is as follows:

$$Ncut(A, B) = \frac{cut(A, B)}{assoc(A, V)} + \frac{cut(A, B)}{assoc(B, V)} \quad (4)$$

where A and B are sub-groups of V:$A \cup B = V$, $A \cap B = \emptyset$; $cut(A, B) = \sum_{u \in A, v \in B} w(u, v)$ is the total weight of edges between A and B; $assoc(A, V) = \sum_{u \in A, t \in V} w(u, t)$ is the total weight of edges within A and $assoc(B, V)$ is the similarly total weight of edges within B.

In practice, spectral clustering can be accomplished by solving a relaxation of the normalized min-cut problem on the graph by using graph Laplacian (Von Luxburg 2007). In this study, we used a normalized graph Laplacian matrix, i.e., $L = I - D^{-1}W$, where the degree matrix $D$is the diagonal matrix with node degrees $d_1, \ldots, d_n$on the diagonal (Shi and Malik 2000). In this case, the first k smallest eigenvectors of L approximates the optimal normalized cut solution to partition the graph into k subsets. In this paper, the second smallest eigenvector of L based clustering method is used to bi-partition the graph into k optimal clusters. By recursively partitioning the sub-graph into two parts according to the second eigenvector and the N-cut value, the optimal graph partition results are achieved. This recursive two-way N-cut algorithm applied in our paper is summarized below (Shi and Malik 2000; Chen et al. 2013).

Input: Functional connectivity matrix W, the threshold of *N-cut: T*

Output: Cluster index of each data point.

1. Compute the normalized graph Laplacian L.
2. Obtain eigenvectors with the smallest eigenvalues.
3. Use the eigenvector with the second smallest eigenvalue to bi-partition the graph.
4. Compare *N-cut* value with T to decide if the current partition need be subdivided.
5. Recursively repartition the segment part until all the partitions cannot be subdivided.

Multi-view Co-training

According to "Temporally dynamic functional connectomes" section, by using the DTI and R-fMRI data, a group of resting-state temporally dynamic functional connectome patterns represented by the corresponding 358 × 358 functional connectivity matrices can be obtained. We applied a spectral graph based multi-view co-training approach here, trying to maximize the functional connectome agreement across temporal patterns (Blum and Mitchell 1998; Kumar and Daumé 2011; Chen et al. 2013). Each pattern/matrix is considered as one view/source of the whole-brain functional connectome and the multi-view co-training procedure tries to obtain more consistent and stable clusters (networks) of the resting state brain.

As described in "Spectral clustering" section, the spectral clustering solves a relaxed version of the min-cut problem and the graph Laplacian matrix is used for its solution. In that case, the first k eigenvectors of the graph Laplacian contain important discriminative information about the clusters, which is utilized in the multi-view spectral clustering in the same way, i.e., we can appropriately employ the eigenvectors from one view to label or constraint the points in other views. An effective indirect approach is introduced here to achieve this goal. Briefly, for the $n \times n$ similarity matrix W, each column w_i can be considered as an n-dimensional vector indicating the similarities between the i-th data point and all n number data points. Besides, the eigenvectors of the generalized graph Laplacian obtained from W are also vectors in the n-dimensional space and the first k eigenvectors have adequate clustering discrimination information as mentioned above. Thus, we can project all the similarity vectors along the k directions (eigenvectors), aiming to retain the inter-cluster discrimination information and ignore the information of within-cluster details. If the projection matrix is orthogonal, an inverse-project operation can be easily implemented to get back the modified similarity matrix. By utilizing this, the similarity graph from each view can be trained and improved by the eigenvectors of the graph Laplacian from the other views based on the projection and inverse-projection procedure. Simply, the projection operation could be defined as:

$$\mathrm{Proj}\,(W, U) = (UU^T W + (UU^T W)^T)/2 \tag{5}$$

where $U \in R^{n\times k}$ is the first k eigenvectors of the graph Laplacian of W. Noted that there is a symmetrization operator to guarantee the symmetry of the modified similarity matrix. Then, *for* m-number views clustering, the multi-view co-training procedure can be accomplished by recursively executing the following *group* projection operation based on Eq. 5:

$$\begin{aligned}\mathrm{Gproj}(W_i) &= \sum_{j=1, j\neq i}^{m} \mathrm{Proj}(W_i, U_j) \\ &= \left(\left(\sum_{j=1, j\neq i}^{m} U_j U_j^T\right) W_i + \left(\left(\sum_{j=1, j\neq i}^{m} U_j U_j^T\right) W_i\right)^T\right)/2\end{aligned} \tag{6}$$

where W_i is the similarity matrix of view i; $U_j \in R^{n\times k}$ is the first k eigenvector matrix of view j. In Eq. 6, the similarity matrix W_i in each view will be updated and improved by the first k eigenvectors of the rest views. After the group projection procedure, the intra-cluster connections in each view will be increased and the inter-cluster connections will be decreased conversely (Chen et al. 2013). The above transformation implies that clustering in each view will be constrained by all of other views. Details of the multi-view co-training procedure were described in Chen et al. 2013.

After an appropriate number of multi-view co-training iteration steps, the final similarity matrix representing the optimal functional connectome between DICCCOLs will be generated by averaging all the m number of revised similarity matrices. With that, using the two-way normalized cut algorithm in "Spectral clustering" section, a set of DICCCOL clusters can be acquired, based on which several dynamic RSNs will be identified and investigated.

Importantly, to compare the difference between the conventional static analysis method and our temporally dynamic analysis method, the multi-view clustering approach was performed on whole-brain temporally dynamic patterns

Input: Functional connectivity matrices of m number views $W_1^0,...,W_m^0$, number of eigenvectors used in projection: k.

Output: Co-trained connectivity matrices $W_1^*,...,W_m^*$.

1. Compute the corresponding initial normalized graph Laplacian matrices $L_1^0,...,L_m^0$ of $W_1^0,...,W_m^0$, and the first k eigenvectors $U_1^0,..,U_m^0$ with smallest eigenvalue of $L_1^0,...,L_m^0$.
2. **for** p=1 to *iter* **do**

(1) $W_i^p = ((\sum_{j=1,j\neq i}^{m} U_j^{p-1}U_j^{p-1T})W_i^{p-1} + ((\sum_{j=1,j\neq i}^{m} U_j^{p-1}U_j^{p-1T})W_i^{p-1})^T)/2$ (i=1,…,m)

(2) Compute the new graph Laplacian and the corresponding first k eigenvectors $U_1^p,..,U_m^p$ of $W_1^p,...,W_m^p$;

end

3. **return** $W_1^* = W_1^p,...,W_m^* = W_m^p$.

("Temporally dynamic functional connectomes" section) and static whole-brain functional connectivity matrices from each resting state subject ("Temporally static functional connectome matrix" section) respectively, by treating each temporal pattern or each static connectivity matrix of single brain as one view of the brain functional connectomes, to obtain two corresponding groups of resting state networks: dynamic multi-pattern clusters and static multi-subject clusters.

Results

Data Acquisition and Pre-processing

Twenty-six healthy adolescents (ages from 11 to 17) participated in this study, under the IRB approvals of the Second Xiangya Hospital and the Central South University, China. Multimodal DTI and resting state fMRI datasets were acquired on a 3T MRI scanner in the West China Hospital, Huaxi MR Research Center, Department of Radiology, Chengdu, China. The acquisition parameters for both scans were as follows. DTI: 256 × 256 matrix, 3 mm slice thickness, 240 mm FOV, 50 slices, 15 DWI volumes, b-value = 1000; R-fMRI: 64 × 64 matrix, 4 mm slice thickness, 220 mm FOV, 30 slices, TR = 2 s. The total scan time of the resting state fMRI dataset is 200 s, i.e. 100 time points. The preprocessing steps can be found in our recent publications (Zhu et al. 2012; Zhang et al. 2012, 2013).

Resting-State Temporally Dynamic Functional Connectome Patterns

By using the methods in "Temporally dynamic functional connectomes" section, totally 474 resting state WQCP samples from 26 adolescents subjects were pooled together for the FDDL learning after a series of processing steps: R-fMRI signal extraction of DICCCOLs, temporally dynamic functional connectivity strength calculation, and segmentation of quasi-stable time periods for each single brain. To determine the optimal number of the potential classes of the training WQCP samples, the Bayesian Information Criterion (BIC) (Schwarz 1978) theory was used. The BIC is defined as:

$$BIC = n \cdot \ln(\sigma_e^2) + k \cdot \ln(n) \quad (7)$$

where σ_e^2 is the error variance, and in this study it is estimated by the summed variance of each WQCP sample within its corresponding class. Here n is the total number of WQCP training samples, and k is the number of learned classes or sub-dictionaries. Generally, given any two estimated models, the model with the lower BIC value is the

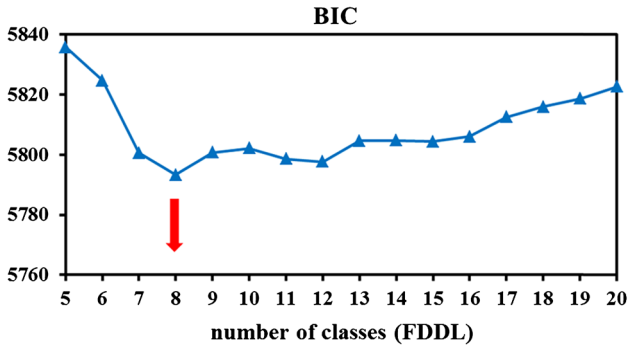

Fig. 5 The corresponding BIC values for different class numbers in the FDDL learning. The minimum of BIC occurs at 8, indicating that the optimal number of classes is 8

one to be preferred. This study tried to calculate the BIC values of the FDDL model using different class numbers (from 5 to 20 in Fig. 5) and determined the number that has the lowest BIC value as the optimal number. For our resting state data, the minimize BIC is acquired when k equals to 8 (Fig. 5).

Thus, totally eight classes emerged after the FDDL classification and the 8 corresponding resting-state temporally dynamic functional connectome patterns were subsequently represented by eight corresponding 358 × 358 DICCCOL-based functional connectivity matrices (Fig. 6). In Fig. 6, each temporal pattern is color-coded based on the same color bar on the right of the figure, ranging from 0 to 1. The magnitude of each element represents the functional connectivity strength between each pair of DICCCOLs. The diagonal elements of each matrix represent the self-connectivity of each DICCCOL, thus equal to 0. It is obvious that this matrix is symmetric and non-negative and can be used as the similarity matrix of DICCCOLs required in the spectral clustering.

From Fig. 6, it can be observed that each temporal pattern has a different functional connectivity strength distribution across different DICCCOL pairs, i.e., different spatial distributions on the brain. This kind of connectivity strength discrimination information across different DICCCOL landmarks in each pattern will have important implications on the true underlying resting-state dynamic functional information interaction of the brain. By deeper investigations into the dynamic functional connection changes among different DICCCOL regions, a group of consistent dynamic resting state networks can be acquired.

Further, to validate the dictionary learning results obtained from WQCP, we resampled 355 (75 %) number of samples out of the total 474 WQCPs for 100 times. In each sampling dataset consisting 355 connectivity strength vectors, we performed the FDDL learning on the dataset in similar steps as described above using the same model parameters (i.e. number of classes and regularization coefficients) to obtain the similar eight functional connectome patterns. Then we compared the connectome patterns obtained from the reduced dataset with connectome patterns from the original full dataset in each of the 100 samplings to see whether each pair of them is similar. The results show that averagely 6 out of 8 connectome patterns obtained from reduced dataset are largely in accordance (relative difference <10 %) with the patterns from the original full dataset. Considering the fact that we were "forcing" the FDDL to learn eight classes from much fewer WQCPs, the comparison result is reasonably good and shows that the functional connectome patterns were not obtained by chance nor artifacts from specific subjects,

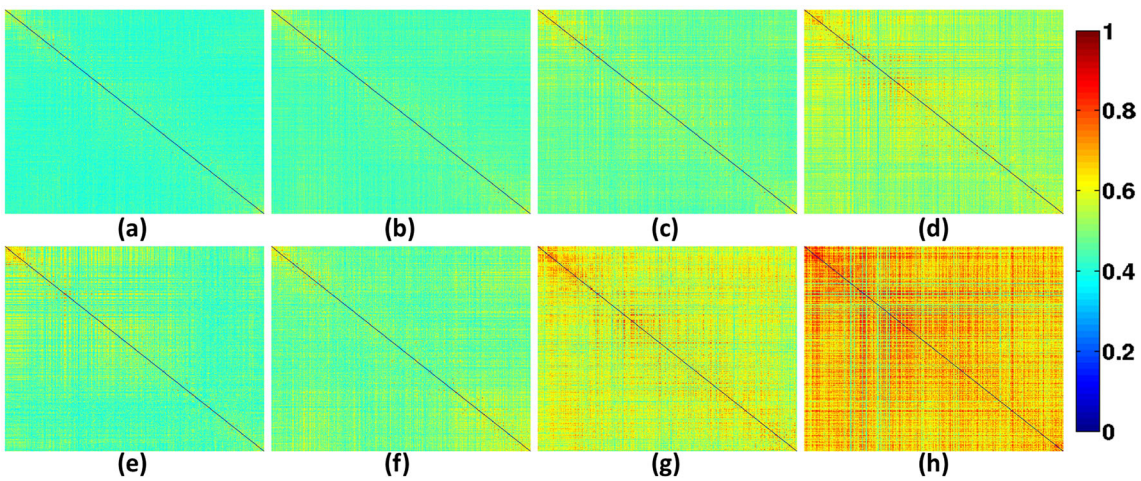

Fig. 6 Eight DICCCOL-based temporally dynamic functional connectome patterns

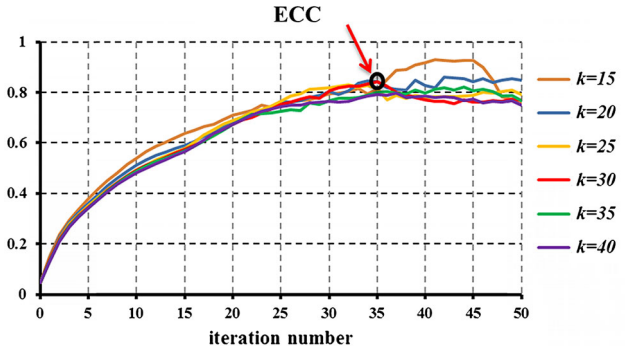

Fig. 7 The Entropy Correlation Coefficient (ECC) values at each multi-pattern co-training iteration step (0–50). Here 0 represents the original similarity matrices. The corresponding ECC *curves* were drawn in different colors respectively for using the first *15, 20, 25, 30, 35, and 40* eigenvectors. When the first 30 eigenvectors were used, the optimal iteration number is determined to be 35 where the highest ECC was obtained and the oscillation occurred after that

and that the dictionary learning results are statistically valid.

DICCCOL-Based Resting State Networks

According to "Identification of DICCCOL-based resting state brain networks", we first applied the multi-view spectral clustering method on eight resting-state temporally dynamic functional connectome patterns to obtain the dynamic resting-state multi-pattern clusters (Fig. 9a, c). Similarly, static multi-subject clusters were also acquired through multi-view spectral co-training on all the static functional connectivity matrices from twenty-six subjects (Fig. 9b, d).

Parameters in Multi-view Co-training

There are two important parameters to be determined during the multi-view co-training, that is, the number of the first k eigenvectors and the number of iterations. As indicated in "Identification of DICCCOL-based resting state brain networks", during the multi-view co-training procedure, the similarity matrix in each view will be modified by projecting to the first k eigenvectors of the graph Laplacian matrix of other views. In general, the value of k should not be less than the true cluster number; otherwise the first k eigenvectors will not contain enough discrimination information for clustering. In other words, some useful information will be removed, resulting in a possible over-training result if we use small k values. On the other hand, if the k is set to be a large number, too much information including the within-cluster details will be retained and an under-training result would be achieved (Chen et al. 2013). In this study, considering the number of our data points, i.e., DICCCOL landmarks, is 358, the first 30 eigenvectors were empirically used in the co-training (the red curve in Fig. 7).

One normalized mutual information measurement called Entropy Correlation Coefficient (ECC) was employed in this study to determine the number of co-training iterations by measuring the agreement between the similarity matrices after each iteration of training (Maes et al. 1997; Chen et al. 2013). The definition of ECC is:

$$ECC(A,B) = \frac{2I(A,B)}{H(A)+H(B)} \tag{8}$$

where $H(A)$ and $H(B)$ are the entropy of matrix $A$and matrix Brespectively and $I(A, B)$is the mutual information between matrices $A$and B. The value of ECC ranges from 0 to 1 and the higher the ECC value is, the more agreement the multi-view training will achieve. Figure 7 shows the ECC value variation curves using different numbers of the first k eigenvectors (*15, 20, 25, 30, 35, and 40*) for multi-pattern clustering. The horizontal axis is the iteration number from 0 to 50, and 0 means the original untrained status. From this figure, it can be noted that as the number of iteration increased, the ECC value first quickly increased and subsequently increased at a reduced speed, then began to oscillate. It means that if too many iteration steps were performed, the multi-view co-training result may become unreliable, e.g., some useful group-wise information may be smoothed. Therefore, an optimal iteration number should be selected more carefully and better to hold a high enough ECC value, while avoiding running into the oscillation part (Chen et al. 2013). For multi-pattern clustering, when the first 30 eigenvectors were selected for co-training (the red curve in Fig. 7), the optimal iteration number is determined to be 35 (pointed by the red arrow in Fig. 7), at which the highest ECC value was obtained and the oscillation appeared after that. Similarly, for multi-subject clustering, the optimal iteration number is determined to be 36.

After multi-view co-training, the final co-trained functional connectivity matrix (similarity matrix) was shown in Fig. 8. The left is from temporally dynamic multi-pattern co-training and the right is from temporally static multi-subject co-training. It can be found that after co-training, the agreement between different views will be substantially increased (e.g., the yellow circles in Fig. 8) and the disagreement will be substantially decreased (e.g., the green circles in Fig. 8). In general, the co-trained matrix is more

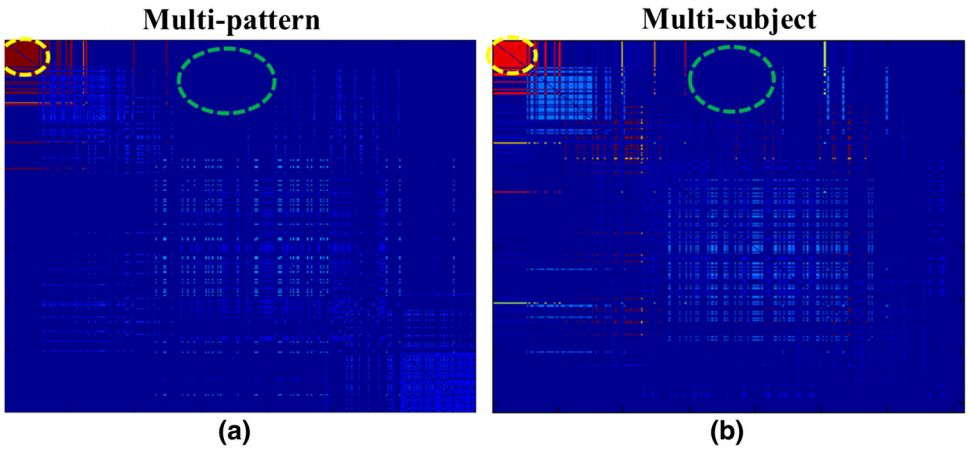

Fig. 8 Modified similarity/connectivity matrix after multi-view co-training for multi-pattern clustering and multi-subject clustering respectively **a** The co-trained multi-pattern clustering matrix, **b** the co-trained multi-subject clustering matrix. After co-training, the agreement between different views will be substantially increased (the *yellow dash circles* in **a** and **b**) and the disagreement will be substantially decreased (the *green dash circles* in **a** and **b**) (Color figure online)

effective and efficient for further clustering than the original single functional connectivity matrix.

The Number of Clusters

During the two-way normalized-cut spectral clustering procedure, the allowed maximum N-cut threshold is adopted to determine whether the sub-graph should be further divided. Generally, the bigger the N-cut threshold is, the more sub-graphs will be considered to be sub-divided and the more clusters will be obtained. In that case, more within-cluster details may be overused. On the other hand, spectral clustering attempts to minimize the N-cut value to achieve the optimal clustering groups. Thus, the N-cut threshold cannot be too large or too small (Chen et al. 2013). Table 1 gives the corresponding cluster numbers when different N-cut thresholds were selected, namely, 0.05, 0.1, 0.2, 0.3, 0.4 and 0.5, respectively. For multi-pattern clustering, the cluster numbers would be nine for 0.05 and 0.1, and ten for 0.2, 0.3, 0.4 and 0.5. For multi-subject clustering, the numbers of clusters would be six for 0.05, eight for 0.1, 0.2, 0.3 and 0.4, and nine for 0.5. In this paper, we selected 0.2 as the final N-cut threshold. Accordingly, totally ten dynamic resting state clusters were obtained from multi-pattern clustering (Fig. 9a) and eight static clusters emerged from multi-subject clustering (Fig. 9b). Furthermore, the DICCCOL groups corresponding to each cluster are visualized on the cortical surface using different color spheres (Fig. 9c, d).

Especially, we also show the functional connectivity strength distributions of the ten DICCCOL clusters in each dynamic temporal pattern by reordering the temporally dynamic functional connectivity matrices in Fig. 6 according to the clustering results shown in Fig. 9a. It can be concluded that the ten clusters are the group-wise optimal clustering results of the eight patterns. The intra-cluster connectivity strengths between DICCCOLs are relatively high and the inter-cluster connectivity strengths are relatively low, especially in the first two patterns (Fig. 10a, b), which hold a higher proportion compared to other patterns, i.e., the most common patterns in resting state. There exist some high inter-cluster functional connectivities in some patterns which may be caused by the influence of the dynamic information interaction changes among spatial regions during certain time periods.

Since each cluster is composed of several DICCCOL landmarks, corresponding to different brain spatial regions, a new measurement was defined based on DICCCOLs to compare the two types of clusters, i.e., the cluster similarity:

$$S(p,q) = \sqrt{\frac{M_{pq}^2}{N_p \cdot N_q}} \; (p = 1, 2, \ldots, 10; q = 1, 2, \ldots, 8) \quad (9)$$

where M_{pq} represents the number of overlapped DICCCOLs between dynamic multi-pattern cluster p and static multi-subject cluster q. N_p and N_q are the total numbers of DICCCOLs in dynamic cluster p and static cluster q respectively. Thus, the cluster similarity will range from 0 to 1, and the higher the cluster similarity is, the more similar the two clusters are. The cluster similarity between each pair of dynamic cluster and static cluster was calculated using the above equation and the result is summarized in Table 2. For each dynamic cluster, the static cluster with the highest similarity (e.g. close to 1) has the highest possibility to be the same brain network or play a similar

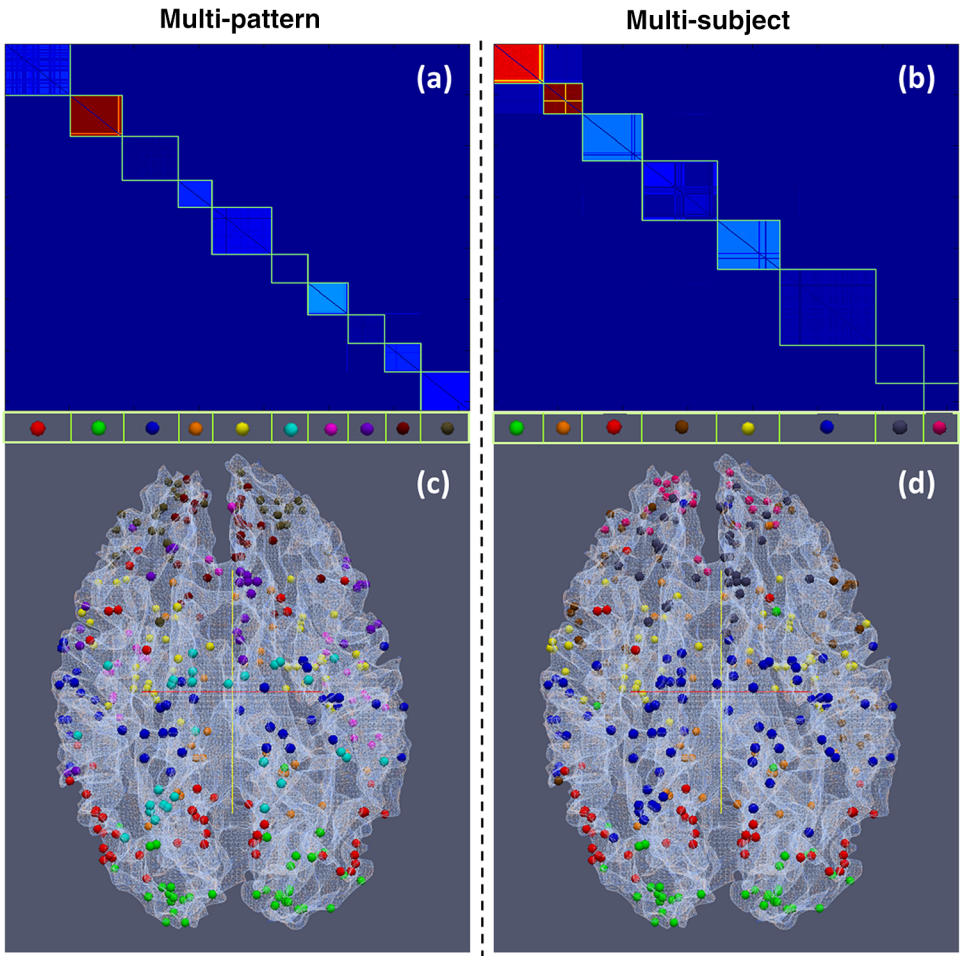

Fig. 9 The DICCCOL clusters/networks derived from the multi-view spectral clustering. **a**, **c** Multi-pattern clustering results; **b**, **d** multi-subject clustering results. In (**a/b**), each cluster is represented by a group of *color spheres* located on the cortical surface in (**c/d**) (Color figure online)

role in resting-state functional interaction. Thus, it is considered as the corresponding cluster of this dynamic cluster (highlighted in bold in Table 2). In Table 2, the dynamic clusters were ranked by the cluster similarity between their corresponding static clusters from high to low and denoted by D1, D2,…, D10, respectively. The corresponding static clusters were denoted by S1, S2,…, S8. In the following part, the clusters, i.e. spatial networks will be analyzed one by one according to their cluster similarities.

Analysis of Resting State Networks

To further understand the spatial distributions of each network on the brain and make our identified networks comparable with reported RSNs in the literature, each DICCCOL landmark's location on a normalized brain was acquired for reference by transforming the corresponding investigated brains into the normalized space, e.g., the MNI space or Talairach space (Yuan et al. 2012). According to Table 2, for each dynamic cluster, the static cluster with the highest cluster similarity with it was selected as its corresponding or associated static cluster, and the detailed comparison of their DICCCOLs or spatial locations were depicted in Fig. 11 and discussed in as follows.

D1 Versus S1 These two clusters (D1 and S1 in Fig. 11a) were the most similar networks among all the dynamic and static clusters with a high similarity of 0.937. By investigations of the spatial locations of the DICCCOLs in this cluster (D1) and previous resting state network studies, it can be inferred that this network is a vision-related resting state network, since it has a large area on the visual cortex regions and shows large overlapping areas with the visual RSNs reported in literature (BAs 17/18/19) (De Luca et al. 2006; Damoiseaux et al. 2006; Sorg et al. 2007; Van den Heuvel et al. 2008). It suggests that the visual resting state network is likely to be the most stable and consistent resting state network of the brain because it exhibits *very* little temporal dynamic changes.

D2 Versus S2 With a high cluster similarity of approximately 0.9, these two clusters (D2 and S2 in Fig. 11b) may indicate a similar network of the resting state brain. This network (D2) mainly contains the parahippocampal gyrus (BAs 30/36) and the hippocampus regions in the

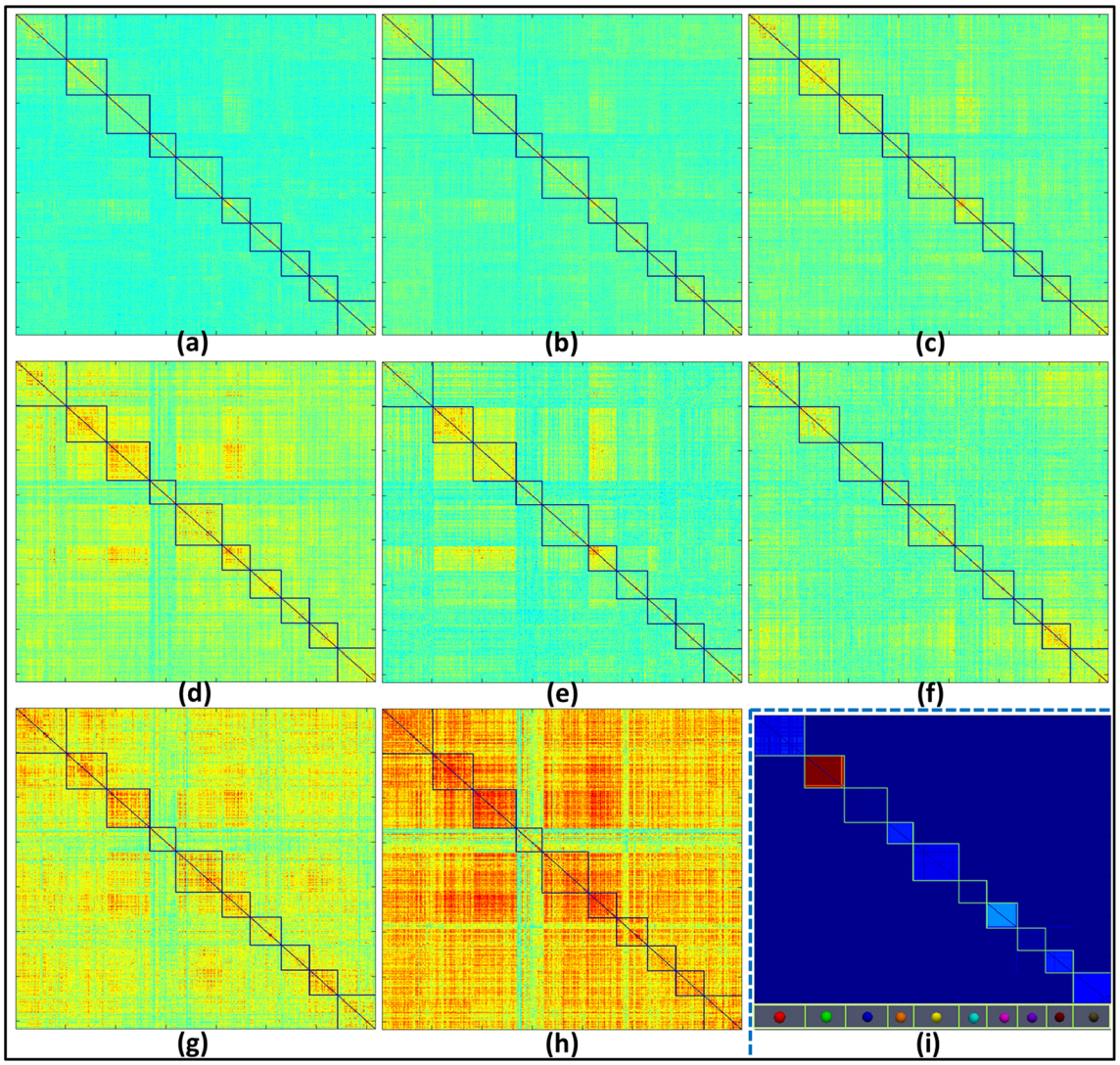

Fig. 10 **a–h** The functional connectivity strength of each dynamic multi-pattern cluster in each temporally dynamic functional connectome pattern corresponding to Fig. 6a–h. **i** multi-patterns clustering results including ten clusters (Fig. 9a)

temporal lobe and limbic lobe and some sub-lobar regions including caudate nucleus, lentiform nucleus and thalamus. *Previous research studies* have shown that both parahippocampal gyrus and hippocampus played an important role in the brain's memory function, such as memory encoding, memory retrieval, episodic memory and spatial memory (Buzsáki et al. 1990; Köhler et al. 2002; Squire and Schacter 2002). Besides, the caudate nucleus has also been demonstrated to participate in the brain's learning and memory system (Packard and Knowlton 2002). Thus, this network may be involved in the memory-related brain activities during resting state, and is likely to be the second most stable and consistent *RSNs* of the brain that exhibits very minor temporal dynamic changes.

D3 Versus S3 The similarity between D3 and S3 clusters (Fig. 11c) is also nearly 0.9. From the locations of DICCCOL points, it is obvious that this network looks quite similar to the generally recognized default mode network (DMN) (Raichle et al. 2001; De Luca et al. 2006; Damoiseaux et al. 2006; Van den Heuvel et al. 2008). This network (D3) was found to have large overlapping regions with the DMN reported in literature, mainly including part of the superior parietal cortex (BA 7) and inferior parietal cortex (BAs 39/40), part of the cingulate cortex including posterior cingulate cortex (BAs 29/30/31), part of the prefrontal cortex (BAs 8/9) and the temporal lobe (BAs 20/21/22/37). Additionally, the stability of DMN at rest can also be confirmed here by the support of high overlapping regions, i.e. high similarity between the temporal dynamics

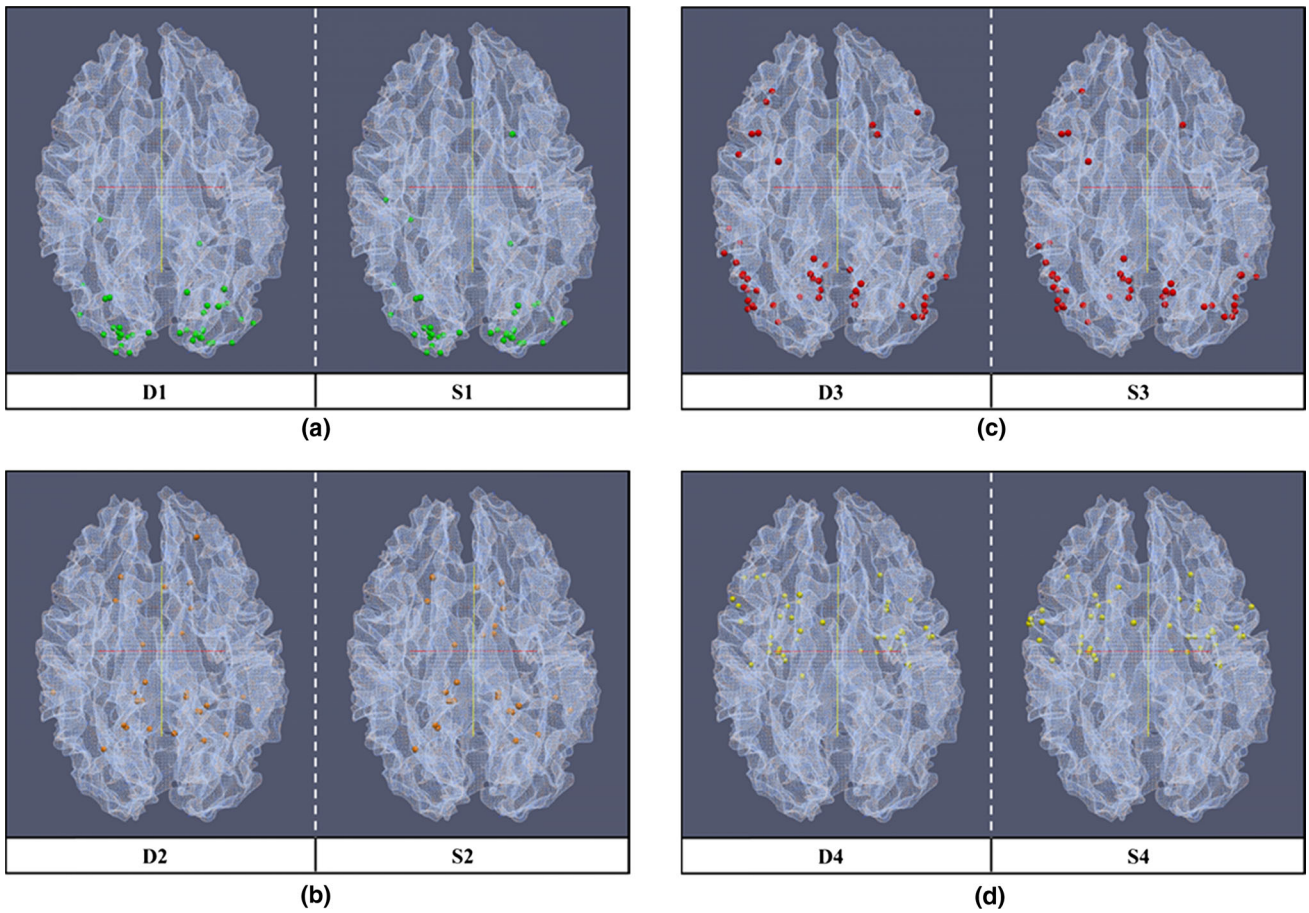

Fig. 11 DICCCOL distributions of the dynamic multi-pattern clusters (D1, D2,…, D10) and the corresponding static multi-subject clusters (S1, S2,…, S8) ranked by the cluster similarity (from high to low). In (**a**–**d**), the dynamic multi-pattern cluster and its corresponding static cluster have a relatively high cluster similarity, thus we use the same *color spheres* for each pair of them. In (**e**) and (**f**), both D5 and D8 correspond to S5, thus we use two types of blue *color spheres*. For (**g**–**j**), the dynamic clusters D6/D7/D9/D10 have relatively low similarity, i.e. many differences exist between them and their corresponding static clusters, thus we use different *color spheres* (Color figure online)

based analysis and the static whole-scan analysis. This result suggests that the DMN is among the most stable and consistent RSNs with only minor temporal dynamic changes. This result also partly explains why the DMN is one of the most reproducible networks in many previous studies.

D4 Versus S4 The similarity between cluster D4 and cluster S4 is also relatively high (0.787). Thus, the large overlapping regions may be a more stable resting state networks but some small areas may exhibit dynamics or variability during the resting state activities of the brain (Fig. 11d). In that case, the dynamic clusters tend to be more accurate to describe the functional interaction between brain networks. This network (D4) mainly includes brain regions such as the bilateral amygdala in the limbic lobe, the lentiform nucleus area composed of the putamen and the globus pallidus, the claustrum and part of insular cortex, part of the frontal lobe containing the precentral gyrus, the inferior and the medial frontal gyrus (BAs 44/45/47) and the superior temporal lobe (BAs 21/22). Regions belonging to this cluster have been verified through task-based fMRI experiments to correspondingly play roles in different kinds of tasks, mostly in memory, movement, semantic and emotional tasks. The specific functions of this cluster, *as well as its connectivity to other clusters*, in resting state need to be further investigated in the future.

D5, D8 Versus S5 Both cluster D5 and cluster D8 have the highest similarity with cluster S5 (Fig. 11e, f). Despite the relatively lower similarities (<0.7), these two dynamic clusters hold most regions of cluster S5 (up to 90 %). For the first network D5, it mainly contains DICCCOLs located in the following regions: superior temporal gyrus (BAs 22/42), postcentral gyrus (BAs 2/3/43) in the parietal lobe, precentral gyrus and medial frontal gyrus (BAs 4/6). The

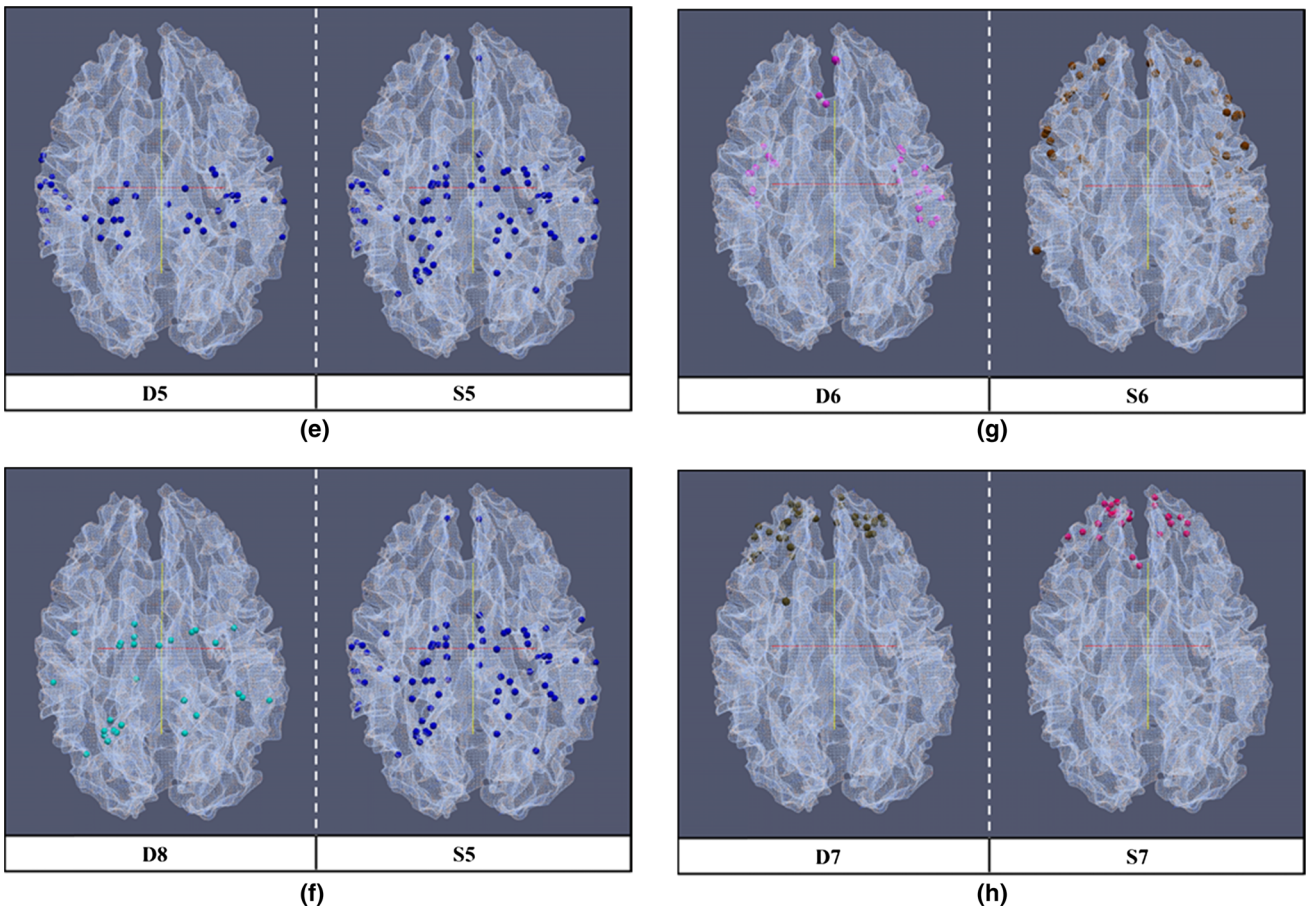

Fig. 11 continued

superior temporal gyrus is so far considered to be higher-order auditory cortex and involved in hearing, speech and etc. As to the other network D8, it is mainly composed of two regions: the precuneus in the superior parietal lobe (BA7) and the precentral gyrus and superior/medial frontal gyrus (BA6) in the frontal lobe. Thus, cluster D6 is likely to be a motor-related RSN. Cluster D5 is also involved in some motor-related activities in some certain degree since it contains part of the motor cortex. The division of D5 and D6 into two different clusters from dynamic multi-pattern clustering indicates that these two networks may participate in different or related functional information processes. The dynamic functional interaction along with time leads to the result that these two dynamic networks correspond to one static network from the view of the whole fMRI scan. However, the accurate functions of these two networks still need to be further investigated in future work.

D6 Versus S6, D7 Versus S7, and D9/D10 Versus S8 The rest of other four dynamic clusters (D6/D7/D9/D10) and their corresponding static clusters (S6/S7/S8) have relatively low similarities (Fig. 11g–j). That is, the differences between each pair of clusters are large. It suggests that clusters D6/D7/D9/D10, as scan time varies, are dynamically interacting with each other during the resting state scan, finally presenting three different resting clusters for the whole time period. Cluster D6 exists in the temporal lobe and covers large parts of the superior, medial and inferior temporal gyrus and the fusiform gyrus (BAs 20/21/22/38). Clusters D7, D9 and D10 cover the majority regions of the frontal lobe. Cluster D7 covers part of the superior, medial and inferior frontal gyrus (BAs 9/10/11); cluster D9 covers part of superior and medial frontal gyrus (BAs 8/9/10) and cingulate cortex (BA 32); cluster D10 covers part of the superior, medial and inferior frontal gyrus and precentral gyrus (BAs 6/9/45/46/47). These results suggest much more temporal function brain dynamics in the frontal lobes. Given the current neuroscience knowledge that the frontal lobes are the major brain regions for higher brain functions *such as attention, working memory and decision making*, our results in this work suggest that there are more temporal dynamics in higher brain functions.

Fig. 11 continued

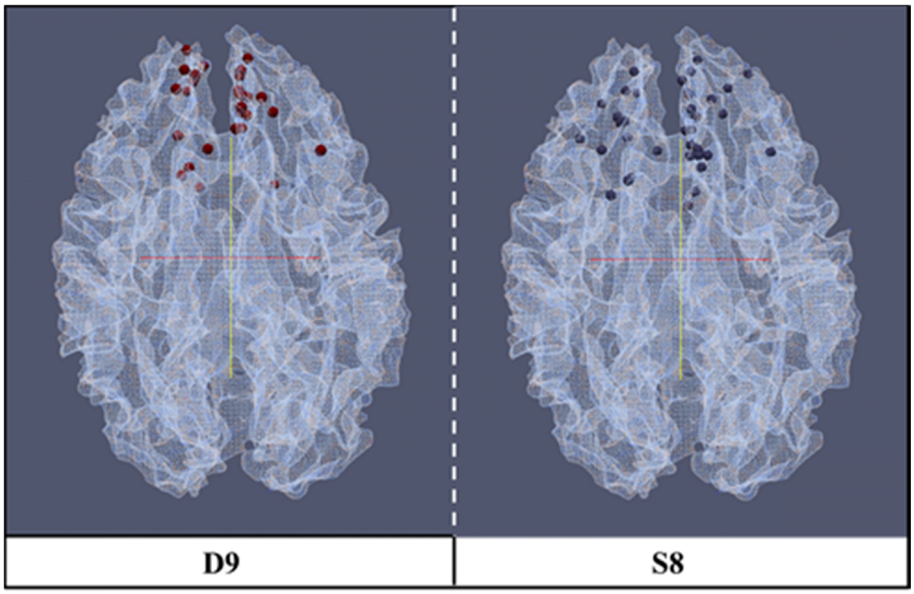

(i)

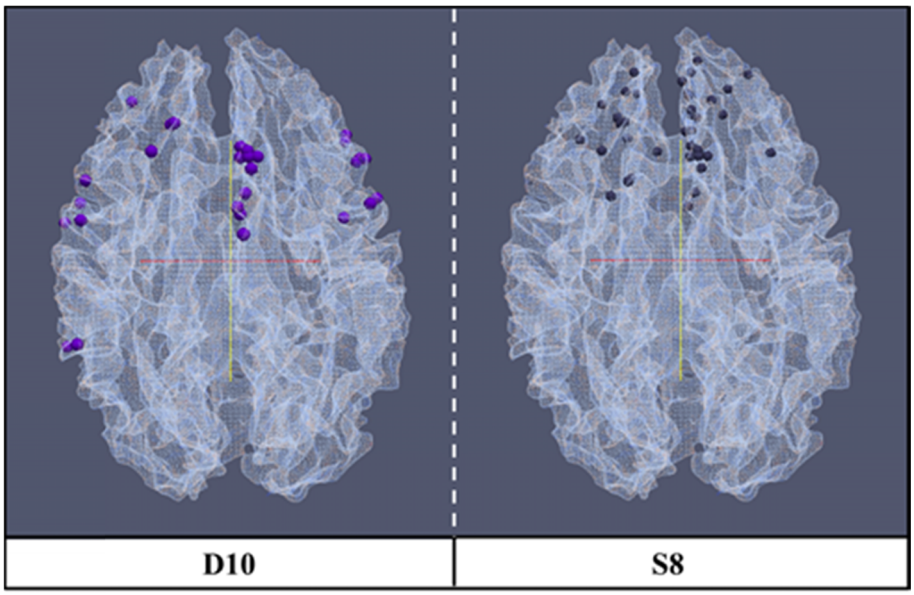

(j)

In summary, the dynamic multi-pattern clustering that makes use of the temporally dynamic information of the brain achieve more clusters (the total cluster number is 10), while the static multi-subject clustering achieve 8 clusters. Interestingly, some of the two types of clusters or networks show high overlapping areas, suggesting these networks are the more stable networks during rest, such as the visual network (D1/S1), the default mode network (D3/S3), and other two networks (D2/S2, D4/S4). The cluster D5 and cluster D8 from multi-pattern method correspond to one static multi-subject cluster S5; D8 covers two important motor cortex regions, the precuneus and the precentral gyrus and appears more relevant to motor RSN; D5 also involves some somatosensory and primary motor regions but with some other regions. Thus it appears that these two clusters might play a different motor-related role in resting state brain activities, but show a similar function in static resting state representation for the whole scan time. Based on further analysis of other four dynamic multi-pattern clusters (D6/D7/D9/D10) in comparison with the other three static multi-subject clusters, it can be inferred that these four networks exhibit much more dynamics and variability. They might play a dynamic coordination role as time varies and present three different static resting state

connectome patterns for the whole time period. In general, our experimental results offer novel insights into the functioning mechanisms of the brain in resting state.

Discussion and Conclusion

This paper presented a novel framework to characterize the temporally dynamics of the brain in resting state. We first utilize the spatial and functional consistence and reproducibility among individual brains based on the large-scale DICCCOL representation system. Then we extract the temporally dynamic functional connectome patterns based on the functional connectivity strength among different DICCCOLs. Subsequently we perform a robust multi-view spectral clustering on these dynamic patterns to obtain a group of relatively stable and consistent dynamic resting state clusters for different temporal patterns. Our work identified a series of resting state networks including the visual RSN, the commonly recognized default mode network, the motor-related RSN and other networks. To compare with the commonly used static methods, a similar multi-view clustering procedure was conducted, and a set of static resting state clusters were obtained. Through the cluster similarity analysis between the dynamic and static clusters, some networks including visual network and default mode network were demonstrated to be the stable RSNs through the whole resting scan time. While some other networks show stronger dynamics and variability during the rest scans. Our result suggests that the temporal dynamics of the brain should be carefully investigated in resting state network studies and more studies should be performed in the future to understand the nature of functional brain dynamics.

Acknowledgments T Liu was supported by the NIH R01 DA-033393, NIH R01 AG-042599, NSF CAREER Award IIS-1149260, and NSF BME-1302089. L Guo was supported by NSFC 61273362 and 61333017. X Zhang and J Lv were supported by the China Government Scholarship and the Doctorate Foundation of Northwestern Polytechnical University. X Hu was supported by the National Science Foundation of China under Grant 61103061, China Postdoctoral Science Foundation under Grant 20110490174 and 2012T50819. Lingjiang Li was supported by The National Natural Science Foundation of China (30830046) and The National 973 Program of China (2009 CB918303).

References

Aertsen AM, Gerstein GL, Habib MK, Palm G (1989) Dynamics of neuronal firing correlation: modulation of "effective connectivity". J Neurophysiol 61(5):900–917

Allen EA, Damaraju E, Plis SM, Erhardt EB, Eichele T, Calhoun VD (2014) Tracking whole-brain connectivity dynamics in the resting state. Cereb Cortex 24:663–676

Assal M, Jagannathan K, Calhoun VD, Miller L, Stevens MC, Sahl R, O'Boyle JG, Schultz RT, Pearlson GD (2010) Abnormal functional connectivity of default mode sub-networks in autism spectrum disorder patients. Neuroimage 53(1):247–256

Beckman CF, DeLuca M, Devlin JT, Smith SM (2005) Investigations into resting-state connectivity using independent component analysis. Philos Trans R Soc Lond B Biol Sci 360(1457): 1001–1013

Bickel S, Scheffer T (2004) Multi-view clustering. Proceeding of the IEEE international conference on data mining

Biswal B, Yetkin FZ, Haughton VM, Hyde JS (1995) Functional connectivity in the motor cortex of resting human brain using echo-planar MR. Magn Reson Med 34(4):537–541

Blum A, Mitchell T (1998) Combining labeled and unlabeled data with co-training. In: Conference on learning theory

Buckner RL, Andrews-Hanna JR, Schacter DL (2008) The brain's default network: anatomy, function, and relevance to disease. Ann N Y Acad Sci 1124:1–38

Buzsáki G, Chen LS, Gage FH (1990) Spatial organization of physiological activity in the hippocampal region: relevance to memory formation. Prog Brain Res 83:257–268

Calhoun VD, Adali T, Pearlson GD, Pekar JJ (2001) A method for making group inferences from functional MRI data using independent component analysis. Hum Brain Mapp 14(3): 140–151

Chang C, Glover GH (2010) Time-frequency dynamics of resting-state brain connectivity measured with fMRI. NeuroImage 50:81–98

Chaudhuri K, Kakade SM, Livescu K, Sridharan K (2009) Multi-view clustering via canonical correlation analysis. In: International conference on machine learning

Chen H, Li K, Zhu D, Jiang X, Yuan Y, Lv P, Zhang T, Guo L, Shen D, Liu T (2013) Inferring group-wise consistent multimodal brain networks via multi-view spectral clustering. IEEE Trans on Med Imaging 32(9):1576–1586

Cordes D, Haughton VM, Arfanakis K, Wendt GJ, Turski PA, Moritz CH, Quigley MA, Meyerand ME (2000) Mapping functionally related regions of brain with functional connectivity MR imaging. AJNR Am J Neuroradiol 21(9):1636–1644

Cordes D, Haughton VM, Carew JD, Arfanakis K, Maravilla K (2012) Hierarchical clustering to measure connectivity in fMRI resting-state data. Magn Reson Imaging 20(4):305–317

Damoiseaux JS, Rombouts SARB, Barkhof F, Scheltens P, Stam CJ, Smith SM, Beckmann CF (2006) Consistent resting-state networks across healthy subjects. Proc Nat Acad Sci USA 103(37):13848–13853

De Luca M, Smith S, De Stefano N, Matthews PM (2005) Blood oxygenation level dependent contrast resting state networks are relevant to functional activity in the neocortical sensorimotor system. Exp Brain Res 167(4):587–594

De Luca M, Beckmann CF, De Stefano N, Matthews PM, Smith SM (2006) fMRI resting state networks define distinct modes of long-distance interactions in the human brain. NeuroImage 29(4):1359–1367

Elad M, Aharon M (2006) Image denoising via sparse and redundant representations over learned dictionaries. IEEE TIP 15(12): 3736–3745

Friston KJ, Frith CD, Liddle PF, Frackowiak RS (1993) Functional connectivity: the principal-component analysis of large (PET) data sets. J Cereb Blood Flow Metab 13(1):5–14

Gembris D, Taylor JG, Schor S, Frings W, Suter D, Posse S (2000) Functional magnetic resonance imaging in real time (FIRE): sliding-window correlation analysis and reference-vector optimization. Magn Reson Med 43:259–268

Gilbert CD, Sigman M (2007) Brain states: top-down influences in sensory processing. Neuron 54(9):677–696

Greicius MD, Krasnow B, Reiss AL, Menon V (2003) Functional connectivity in the resting brain: a network analysis of the default mode hypothesis. Proc Nati Acad Sci USA 100(1): 253–258

Greicius MD, Srivastava G, Reiss AL, Menon V (2004) Default-mode network activity distinguishes Alzheimer's disease from healthy aging: evidence from functional MRI. Proc Nati Acad Sci USA 101(13):4637–4642

Hampson M, Olson IR, Leung HC, Skudlarski P, Gore JC (2004) Changes in functional connectivity of human MT/V5 with visual motion input. NeuroReport 15(8):1315–1319

Jiang T, He Y, Zang Y, Weng X (2004) Modulation of functional connectivity during the resting state and the motor task. Hum Brain Mapp 22(1):63–71

Köhler S, Crane J, Milner B (2002) Differential contributions of the parahippocampal place area and the anterior hippocampus to human memory for scenes. Hippocampus 12(6):718–723

Kumar A, Daumé H (2011) A co-training approach for multi-view spectral clustering. ICML-11

Larson-Prior LJ, Zempel JM, Nolan TS, Prior FW, Snyder AZ, Raichle ME (2009) Cortical network functional connectivity in the descent to sleep. Proc Natl Acad Sci USA 106(11): 4489–4494

Li X, Zhu D, Jiang X, Jin C, Zhang X, Guo L, Zhang J, Hu X, Li L, Liu T (2013) Dynamic functional connectomics signatures for characterization and differentiation of PTSD patients. Hum Brain Mapp. doi:10.1002/hbm.22290

Lowe MJ, Mock BJ, Sorenson JA (1998) Functional connectivity in single and multislice echoplanar imaging using resting-state fluctuations. Neuroimage 7(2):119–132

Maes F, Collignon A, Vandermeulen D, Marchal G, Suetens P (1997) Multimodality image registration by maximization of mutual information. Med Imaging IEEE Trans 16(2):187–198

Mairal J, Elad M, Sapiro G (2008) Sparse representation for color image restoration. IEEE TIP 17(1):53–69

Mairal J, Bach F, Ponce J, Sapiro G, Zisserman A (2009) Non-local sparse models for image restoration. ICCV

Packard MG, Knowlton BJ (2002) Learning and memory functions of the basal ganglia. Annu Rev Neurosci 25:563–593

Raichle ME, Snyder AZ (2007) A default mode of brain function: a brief history of an evolving idea. Neuroimage 37(4):1083–1090

Raichle ME, MacLeod AM, Snyder AZ, Powers WJ, Gusnard DA, Shulman GL (2001) A default mode of brain function. Proc Natl Acad Sci USA 98(2):676–682

Sakoğlu Ü, Pearlson G, Kiehl K, Wang YM, Michael A, Calhoun V (2010) A method for evaluating dynamic functional network connectivity and task-modulation: application to schizophrenia. Magn Reson Mater Phys Biol Med 23:351–366

Schwarz GE (1978) Estimating the dimension of a model. Ann Stat 6(2):461–464

Shi J, Malik J (2000) Normalized cuts and image segmentation. Pattern Anal Mach Intel IEEE Trans 22(8):888–905

Smith SM, Miller KL, Moeller S, Xu J, Auerbach EJ, Woolrich MW, Beckmann CF, Jenkinson M, Andersson J, Glasser MF, Van Essen DC, Feinberg DA, Yacoub ESM, Ugurbil K (2012) Temporally-independent functional modes of spontaneous brain activity. Proc Natl Acad Sci USA 109:3131–3136

Sorg C, Riedl V, Mühlau M, Calhoun VD, Eichele T, Läer L, Drzezga A, Förstl H, Kurz A, Zimmer C, Wohlschläger AM (2007) Selective changes of resting-state networks in individuals at risk for Alzheimer's disease. Proc Natl Acad Sci USA 104(47): 18760–18765

Squire LR, Schacter DL (2002) The neuropsychology of memory. Guilford Press, New York, USA

Starck J, Elad M, Donoho D (2005) Image decomposition via the combination of sparse representation and a variational approach. IEEE Trans Image Process 14(10):1570–1582

Thirion B, Dodel S, Poline JB (2006) Detection of signal synchronizations in resting-state fMRI datasets. Neuroimage 29(1): 321–327

Van den Heuvel M, Mandl R, Hulshoff Pol H (2008) Normalized cut group clustering of resting-state fMRI data. PLos ONE 3(4):e2001

Von Luxburg U (2007) A tutorial on spectral clustering. Stat Comput 17(4):395–416

Wright J, Ma Y, Mairal J, Sapiro G, Huang TS, Yan S (2010) Sparse representation for computer vision and pattern recognition. PIEEE 98(6):1031–1044

Yang J, Yu K, Gong Y, Huang T (2009) Linear spatial pyramid matching using sparse coding for image classification. CVPR

Yang M, Zhang L, Feng X, Zhang D (2011) Fisher discrimination dictionary learning for sparse representation. ICCV

Yuan Y, Jiang X, Zhu D, Chen H, Li K, Lv P, Yu X, Li X, Zhang S, Zhang T, Hu X, Han J, Guo L, Liu T (2013) Meta-analysis of functional roles of DICCCOLs. Neuroinformatics 11(1):47–63

Zhang Q, Li BX (2010) Discriminative K-SVD for dictionary learning in face recognition. CVPR

Zhang X, Guo L, Li X, Zhu D, Li K, Sun Z, Jin C, Hu X, Han J, Zhao Q, Li L, Liu T (2012) Characterization of task-free/task-performance Brain States. MICCAI, Nice, France

Zhang X, Guo L, Li X, Zhang T, Zhu D, Li K, Chen H, Lv J, Jin C, Zhao Q, Li L, Liu T (2013) Characterization of task-free and task-performance brain states via functional connectome patterns. Med Image Anal 17(8):1106–1122

Zhu D, Li K, Faraco CC, Deng F, Zhang D, Jiang X, Chen H, Guo L, Miller LS, Liu T (2011) Optimization of functional brain ROIs via maximization of consistency of structural connectivity profiles. NeuroImage 59(2):1382–1393

Zhu D, Li K, Guo L, Jiang X, Zhang T, Zhang D, Chen H, Deng F, Faraco C, Jin C, Wee CY, Yuan Y, Lv P, Yin Y, Hu X, Duan L, Hu X, Han J, Wang L, Shen D, Miler LS, Li L, Liu T (2012) DICCCOL: dense Individualized and common connectivity-based cortical landmarks. Cereb Cortex 23(4):786–800